

Article

One-Step Methods to Fabricate Durable Superhydrophobic Coatings for Flexible Electronic Sensors

Xiang Liu ¹ , Kai Chen ², Dekun Zhang ^{2,*} and Zhiguang Guo ^{3,4,*}

¹ School of Mechatronic Engineering, China University of Mining and Technology, Xuzhou 221116, China; xiangliu0229@163.com

² School of Materials Science and Physics, China University of Mining and Technology, Xuzhou 221116, China; cumtck@cumt.edu.cn

³ Hubei Collaborative Innovation Centre for Advanced Organic Chemical Materials and Ministry of Education Key Laboratory for the Green Preparation and Application of Functional Materials, Hubei University, Wuhan 430062, China

⁴ State Key Laboratory of Solid Lubrication, Lanzhou Institute of Chemical Physics, Chinese Academy of Sciences, Lanzhou 730000, China

* Correspondence: dkzhang@cumt.edu.cn (D.Z.); zguo@licp.cas.cn (Z.G.)

Abstract: Inspired by lotus leaves in nature, superhydrophobic surfaces have attracted extensive attention in many fields. However, their complex preparation process, poor durability and high cost seriously restrict their large-scale application in industrial production. Based on the good flexibility and durability of carbon nanofibers, several simple modifier-free one-step approaches were adopted to fabricate a durable CNF/PVDF/PDMS conductive superhydrophobic coating. The fabricated coating not only possesses good superhydrophobicity to many kinds of liquids, but also has excellent self-cleaning and anti-fouling properties. In addition, the superhydrophobicity of the obtained multifunctional coating is stable even after harsh bending fatigue deformation, long immersion times and high-temperature treatment. Due to its strong adhesion and excellent conductivity, the CNF/PVDF/PDMS coating displays reliable mechanical stability and superior sensitivity. These distinct features make the obtained conductive superhydrophobic coating a good candidate for multifunctional smart sensors, with great application prospects in gesture detectors, waterproof wearable electronics and health monitors.

Keywords: one-step methods; durable; superhydrophobicity; flexible; electronic sensor



Citation: Liu, X.; Chen, K.; Zhang, D.; Guo, Z. One-Step Methods to Fabricate Durable Superhydrophobic Coatings for Flexible Electronic Sensors. *Coatings* **2021**, *11*, 95. <https://doi.org/10.3390/coatings11010095>

Received: 21 November 2020

Accepted: 12 January 2021

Published: 16 January 2021

Publisher's Note: MDPI stays neutral with regard to jurisdictional claims in published maps and institutional affiliations.



Copyright: © 2021 by the authors. Licensee MDPI, Basel, Switzerland. This article is an open access article distributed under the terms and conditions of the Creative Commons Attribution (CC BY) license (<https://creativecommons.org/licenses/by/4.0/>).

1. Introduction

With a high water contact angle (WCA, $>150^\circ$), and a low sliding angle (SA, $<10^\circ$), superhydrophobic surfaces, inspired by natural creatures, have attracted extensive attention in academia [1,2]. Many methods, such as electrospinning [3,4], sol-gel [5–7], etching [8–10], hydrothermal [11,12], self-assembly [13,14] and template methods [15,16], have been used to prepare superhydrophobic surfaces. With the development of superhydrophobic technology, a single superhydrophobic surface cannot meet our requirements. Therefore, multifunctional superhydrophobic surfaces are fabricated by combining superhydrophobicity with other properties, such as conductivity [17,18], antimicrobial activity [19], electromagnetic shielding [20] and self-healing [21,22], expanding the application field of superhydrophobic surfaces. As an important development of multifunctional superhydrophobic surfaces, conductive superhydrophobicity has been a new focus of superhydrophobic surfaces. In addition to exhibiting electrical conductivity, conductive superhydrophobic surfaces can work in humid and acid-base conditions, which can greatly extend the service life of surfaces [23].

Flexible durable conductive superhydrophobic surfaces will be widely used in industrial production because of their flexible, convenient and practical characteristics [24,25].

To date, a few studies on flexible conductive superhydrophobic surfaces have been reported [26–28]. As is known, superhydrophobic surfaces depend on two main factors: surface roughness and low surface energy [29,30]. The surface roughness is mainly provided by various surface treatment methods, and low surface energy can be obtained from fluorinated or long chain polymers [31]. Nevertheless, it is well known that polymers generally have high surface resistivity, and the adhesion between polymers and matrices is usually not good [32]. Thus, the preparation of conductive superhydrophobic (CS) surfaces with good conductivity and adhesion to substrate is still a great challenge [33]. In general, CS surfaces are obtained by adding a certain amount of conductive filler to surfaces. The commonly used conductive fillers are metals, metal oxides, carbon materials and conductive polymers [34]. In particular, due to their excellent thermal conductivity and ability to effectively eliminate accumulated static charges, carbon materials have been utilized to prepare conductive superhydrophobic surfaces [35,36]. Lu et al. [37] fabricated robust superhydrophobic surfaces by spraying commercial adhesives between superhydrophobic paint and substrates. Even after finger wiping, knife scraping and 40 sandpaper abrasion cycles, the obtained superhydrophobic surfaces remained superhydrophobic. It provides a way of thinking to the weak point of the superhydrophobic field is handed over to more mature adhesive technology to overcome. Based on the above analysis, it is feasible to fabricate stable and durable conductive superhydrophobic surfaces by using carbon materials and commercial binders. The fabrication of robust CS surfaces using simple methods has good application prospects.

Carbon nanofibers (CNF), a common carbon material, has been widely used in industrial production because of its chemical inertness, low production costs and good bending stability [38]. It also has been used to fabricate CS surfaces due to its excellent conductivity [39]. However, constrained by complex preparation processes, high production costs, and environmental protection, most of the reported CS surfaces are difficult to apply in practical production [40,41]. Therefore, it is very important for superhydrophobic surface applications to prepare low-cost and environmentally friendly superhydrophobic surfaces by simple methods. In fact, coating is the most convenient and universally applicable approach for preparing superhydrophobic surfaces [42]. In this work, three simple one-step methods (brush coating, spraying and dip-coating) were adopted to fabricate conductive superhydrophobic coatings. Compared with common polymer materials, polyimide is a good high-temperature-resistant material with excellent mechanical, radiation and solvent resistance properties, so it is a good candidate material for the preparation of flexible substrates [43]. To improve adhesion between a coating and a substrate, polyimide (PI) tape was selected as the flexible substrate. The obtained CS coating was composed of CNF, PDMS and PVDF. CNF, producing multi-scale microstructures and thus, rough surfaces, were selected as conductive fillers to prepare flexible wearable conductive superhydrophobic coatings. Polydimethylsiloxane (PDMS), as the binder, as well as polyvinylidene fluoride (PVDF), provide the required low surface energy for the CS coating. In addition, PVDF can also combine with CNF to form a multi-scale micro/nano-composite structure, which provides roughness support for superhydrophobic surface formation. These multiple simple one-step methods with low production costs can meet the needs of various industrial production processes. It is believed that the processes elaborated in this article possess certain practical application value and reference significance for superhydrophobic research.

2. Experiment

2.1. Materials

Polyimide tape was obtained from Shenzhen Hongzhan Adhesive Technology Co., Ltd. (Shenzhen, China). CNF (20–200 μm -long and 100 nm in diameter) were purchased from Sigma-Aldrich Co., Ltd (Saint Louis, MI, USA). Polyvinylidene fluoride power was supplied by Arkema Kynar Co., Ltd. (Paris, France). Terpeneol was obtained from Xilong Science Co., Ltd. (Shantou, China). Polydimethylsiloxane was provided by Dow Sili-

cones Corporation (Midland, MI, USA). The other reagents were used as received without further purification.

2.2. Preparation of the Flexible Conductive Superhydrophobic Coating

At room temperature, 0.1 g CNF and 0.1 g PVDF were added into 2.5 g terpineol to form a uniform dispersion solution after enough stirring. Subsequently, 0.1 g PDMS and 0.01 g curing agent were added into the above homogeneous solution in turn, ultrasonically dispersed and adequately agitated to form well dispersed paint.

Multiple simple methods were adopted to fabricate the conductive superhydrophobic composite coating. First, the brush coating method can be used to prepare a flexible conductive superhydrophobic coating (FCS coating). The well dispersed paint was evenly applied to the PI tape surface with a homemade brush. At room temperature, the brushed sample was placed in a petri dish for 30 min to let the paint level. Second, the spraying method can also be adopted to fabricate the FCS coating. Before spraying, PI tape (30 mm × 20 mm, sticky side up) was fixed to cardboard with double-sided tape. Afterwards, the above prepared paint was sprayed onto the polyimide tape surface using the 1.0 MPa N₂ gas spray gun. During the spraying process, the spray gun was at a 45° angle with the sample, and the nozzle was about 15 cm away from the sample. The spraying time lasted for 3 s, and then the samples were dried in a 100 °C oven for 10 min. After spraying three times, the paint can completely and evenly cover the substrate surface. Finally, the FCS coating can be fabricated by the dip-coating method. The PI tape was immersed in the paint for 10 s and then slowly removed. After that, the removed samples were dried at 100 °C for 10 min. The FCS coating can be obtained after 5 times of dip-coating. The coatings obtained by the above three methods were cured at 230 °C for 10 min. A schematic diagram of the preparation process used for the FCS coating is shown in Figure 1.

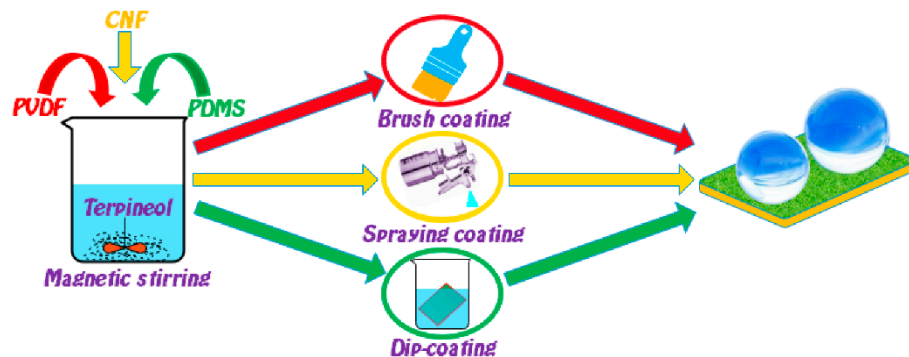


Figure 1. Schematic diagram of the preparation process of the flexible conductive superhydrophobic coating.

2.3. Characterization

The surfaces of the specimens were sputtered with Au before testing and observed by field emission scanning electron microscopy (FESEM, JSM-6701F, Japan Electronics Co., Tokyo, Japan, measured current of 10 μ A, accelerating voltage of 5 kV). Fourier transform infrared spectroscopy (FTIR, Nexus 870, Thermo Fisher Scientific, Waltham, MA, USA) was employed to analyze the chemical compositions in the measuring range of 4000–400 cm^{-1} . The WCAs and SAs were measured with 5 and 8 μ L deionized water droplets, respectively, on a contact angle (CA) system (JC2000D1CA meter, Shanghai Zhongchen, Shanghai, China). The average values of WCAs and SAs were obtained by measuring five different regions of the sample. The element distribution and chemical compositions were analyzed by energy-dispersive X-ray spectroscopy (EDS, JSM-5600LV, Japan Electronics Co., Tokyo, Japan). A resistivity meter (MCP-T610, Mitsubishi, Tokyo, Japan) with a four-point probe was used to measure the electrical conductivity of samples with differently modified CNF contents. The normalized relative resistance was measured by using a digital multimeter (EM33D, Elecall, Wenzhou, China). A precision roughness tester (JB-4C, Shanghai Precision

Instrument Co., Shanghai, China) was utilized to measure the CS surface roughness. The average values of all data were obtained by measuring five different regions of the sample. The average values of all the results in this paper were obtained by measuring five groups of test data.

3. Results and Discussion

3.1. Fabrication of the FCS Coating

To determine the best parameters for processing the coating, variations in superhydrophobicity, surface roughness and surface resistivity obtained with different additive contents were investigated by using the control variable method. In Figure S1a,d,g, it can be easily seen that the WCAs increase first and then decrease with increasing CNF content, which is similar to the change trend of roughness and opposite to that of SAs obtained with different CNF contents. The above results are consistent with Wenzel's theory. Increasing the surface roughness is beneficial for improving the hydrophobicity of the coating. When the CNF amount is more than 0.1 g, the surface superhydrophobicity is not improved by increasing roughness, which can be explained by the fact that excessive carbon fibers can increase the surface energy of the coating. Similar phenomena can also be found at different PVDF contents (Figure S1c,f). In addition, increasing the CNF content can reduce the surface resistivity because of the formation of a conductive path, as shown in Figure S1g. However, at 0.20 g CNF, the excessive CNF cannot be evenly dispersed in the coating, which damages the conductive path and then increases the surface resistivity. In Figure S1i, the surface resistivity increases with increasing PVDF content, which is attributed to the poor conductivity of the polymer (PVDF). At different PDMS contents (Figure S1b,e), the WCAs increase first and then decrease with increasing PDMS contents, which is contrary to the change trend of roughness. The above phenomenon can be attributed to the low surface energy and good adhesion of PDMS. In the initial stage, the increase in the amount of PDMS uniformly coated on the particle surface can reduce the surface energy of the coating and improve the superhydrophobicity. Meanwhile, it can also reduce the surface roughness. When the PDMS amount is more than 0.1 g, the particles in the coating will agglomerate with the addition of PDMS, which can affect the dispersion of the coating. Therefore, the roughness increases with increasing PDMS content due to the agglomeration of particles, which affects the microstructure of the superhydrophobic surface. In Figure S1h, the surface resistivity increases with the increasing PDMS content because of its poor conductivity. With the further increase in PDMS content above 0.05 g, the surface resistivity of the coating decreases and tends to be stable, which can be explained by the fact that the conductive path of the coating is more compact due to the adhesiveness of PDMS.

Accordingly, it can be concluded that an appropriate surface roughness is indispensable for the preparation of superhydrophobic coatings. Based on the above analysis results, the optimal parameters for obtaining superhydrophobicity (157.5° WCA, 5.3° SA) on the coating surface are 0.1 g CNF, 0.1 g PDMS and 0.1 g PVDF. Table S1 shows the surface resistivity and logarithmic values of the superhydrophobic coating with different carbon contents (g and wt %). From Table S1 and Figure S1g–i, it is easily seen that the optimal conductivity (339Ω) can be obtained on the coating surface when the CNF amount is 0.15 g. Furthermore, the WCA is 149.3° and the SA is 9.9° , which indicates that the superhydrophobicity achieved with 0.15 g CNF is worse than that achieved with 0.2 g CNF. In addition, the surface resistivity achieved with 0.1 g CNF is 784Ω , which is the same order of magnitude as that achieved with 0.15 g CNF. Considering the factors of superhydrophobicity, conductivity and material savings, the optimal parameters of the FCS coating are 0.1 g CNF, 0.1 g PDMS and 0.1 g PVDF.

The cross-sectional morphology of the coatings prepared by three methods are shown in Figure S2a,c,d. The FCS coating obtained by brush coating (Figure S2a) has a compact cross-section morphology, which may be beneficial to improve the durability of the coating. In contrast, the FCS coatings prepared by spraying (Figure S2c) and dip-coating (Figure S2c) have relatively loose cross-section morphologies, which may be attributed to the multiple

coating processes in the preparation process. Therefore, in this paper, the FCS coating obtained by brush coating is selected for relevant experimental analysis and research. In addition, from Figure S2b, it can be estimated that the thickness of the coating prepared by brush coating is about 40 μm .

Figure 2a shows a digital picture of the paint fabricated with the optimum parameters. It can be clearly seen that the paint, without delamination, is uniformly stored in a transparent sample bottle. Moreover, some paint is adhered on the inner wall of the sample bottle, which indicates that the prepared paint has certain adhesion. The adhesion of the obtained paint is the basis of three one-step methods. After two weeks of storage, the additives are still well dispersed in the obtained paint without obvious delamination (Figure 2b), which illustrates that the prepared paint has good durability and stability. Figure 2c displays the state of different droplets on the coating surface prepared on different substrates. The prepared paint can be applied on different substrates, and the six different droplets maintain spherical shapes on the coating surface, which illustrates that the coating surface has good superhydrophobicity to different droplets.

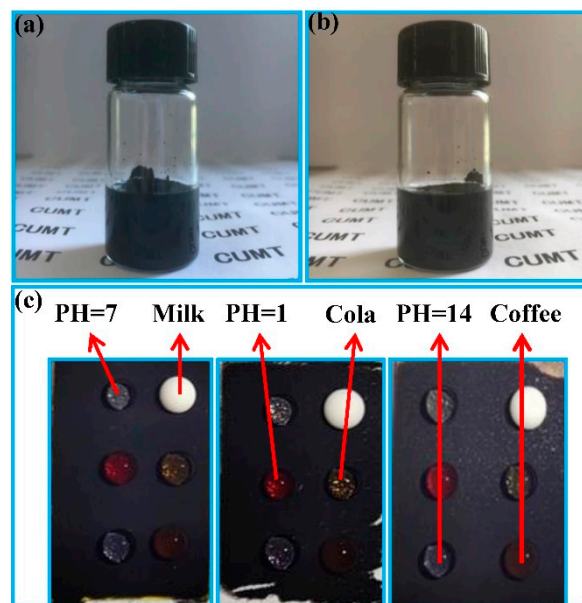


Figure 2. (a) Digital picture of the fabricated paint; (b) digital photo of the paint after two weeks of storage; (c) the states of different droplets on the coating surface prepared on different substrates (from left to right, the three substrates are a polyimide (PI) film, a slide and Q345).

The SEM surface morphologies of the fabricated FCS coating are exhibited in Figure 3a–c. From Figure 3a, it can be clearly seen that the microstructure of the coating is cauliflower-like, and particles with random sizes are evenly distributed on the coating surface. The insets are images showing the WCA (157.5°) and SA (5.3°). In addition, even in the bending state, the water droplets can still easily roll off the coating surface, and a water jet can bounce on the surface without leaving any residual droplets (Movie S1). The above results show that the prepared coating has excellent superhydrophobic properties. The surface roughness curve of the obtained FCS coating is displayed in Figure 3d, and the corresponding roughness value is 0.404 μm . In Figure 3b, particles of different sizes are distributed on the coating surface at intervals to form a random concave and convex microstructure, which provides important structural support for superhydrophobicity. According to Wenzel's theory, air is filled between the concave and convex structures, which reduces the contact area between the surface particles and water droplets, thus improving the superhydrophobicity of the surface. In addition, the CNF are embedded in the coating and show network structures interwoven with each other on the surface

(red circles in Figure 3c). The network structures formed by the CNF can provide good conductive paths for the charges to improve the conductivity of the FCS coating.

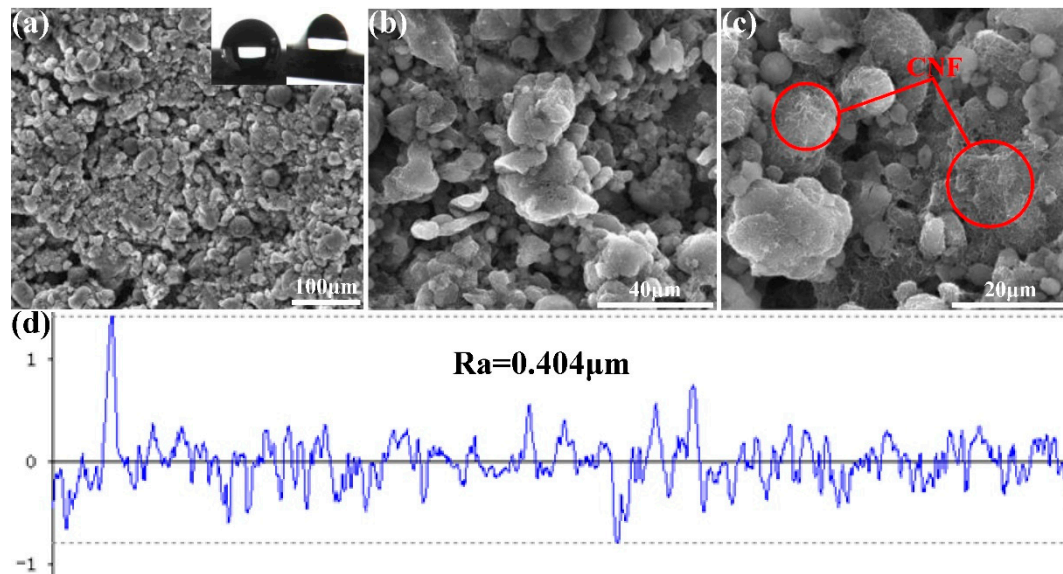


Figure 3. Surface morphologies under different magnifications: ((a) 600× SEM image; (b) 2500× SEM image; and (c) 5000× SEM image). The insets in Figure 3a are images showing the water contact angle (WCA), and a low sliding angle (SA); (d) the surface roughness value and curve of the obtained flexible conductive superhydrophobic (FCS) coating.

Surface energy is a significant factor in the fabrication of superhydrophobic surfaces and it can be calculated by the model proposed by Owens [44]. According to the Owens' model, the liquid surface energy can be expressed as follows:

$$\gamma_{la} = \gamma_l^d + \gamma_l^p \quad (1)$$

where γ_{la} , γ_s^d and γ_s^p are the gas–liquid surface tension, dispersion force and polarity force, respectively. The contact angle of liquid on the smooth solid surface can be expressed by Young's Equation (2):

$$\gamma_{sa} = \gamma_{sl} + \gamma_{la} \cos \theta \quad (2)$$

where γ_{sa} and γ_{sl} correspond to solid–gas and solid–liquid surface tensions, respectively, and θ is the steady contact angle of the smooth solid surface. In this paper, before measuring θ , the superhydrophobic surface should be polished, and then the liquid contact angles were measured on the polished surface. The corresponding liquid contact angles are shown in Table S2. In addition, solid–liquid surface energy can be expressed by the following:

$$\gamma_{sl} = \gamma_{sa} + \gamma_{la} - 2\sqrt{\gamma_s^d \gamma_l^d} - 2\sqrt{\gamma_s^p \gamma_l^p} \quad (3)$$

The relationship between the contact angle and the component forces (Equation (4)) can be obtained by simultaneous Equations (2) and (3):

$$1 + \cos \theta = \frac{2\sqrt{\gamma_s^d \gamma_l^d}}{\gamma_l} + \frac{2\sqrt{\gamma_s^p \gamma_l^p}}{\gamma_l} \quad (4)$$

The dispersion force and polarity force of water and Diiodomethane are displayed in Table S2. After calculation, we can get $\gamma_{sa} = \gamma_s^d + \gamma_s^p = \gamma_s^d = 26.4 \text{ mJ/m}^2$, which is the surface energy of the FCS coating.

The peaks at 1210 and 1176 cm^{-1} in the FTIR spectra of the FCS coating (Figure 4a) are assigned to the $-\text{CF}_2-$ group stretching vibration in PVDF, which provides the low surface

energy essential for the FCS coating. The absorption bands observed at 1400 cm^{-1} should be ascribed to the stretching vibration of $-\text{CH}_2-$ groups. In addition, the bands at 1260 and 796 cm^{-1} correspond to the asymmetric bonds of $\text{Si}-\text{O}-\text{C}$ and $\text{Si}-\text{C}$ in PDMS, reducing the surface energy of the FCS coating. The EDS spectrum in Figure 4b shows that the FCS coating is composed of C, F, Si, and O. The F and Si peaks are attributed to the existence of PVDF and PDMS in the FCS coating, respectively. Moreover, the elemental distribution images are displayed in Figure 4c–f, showing that the elements of various additives are evenly distributed on the coating surface, which corresponds to the result in Figure 4b.

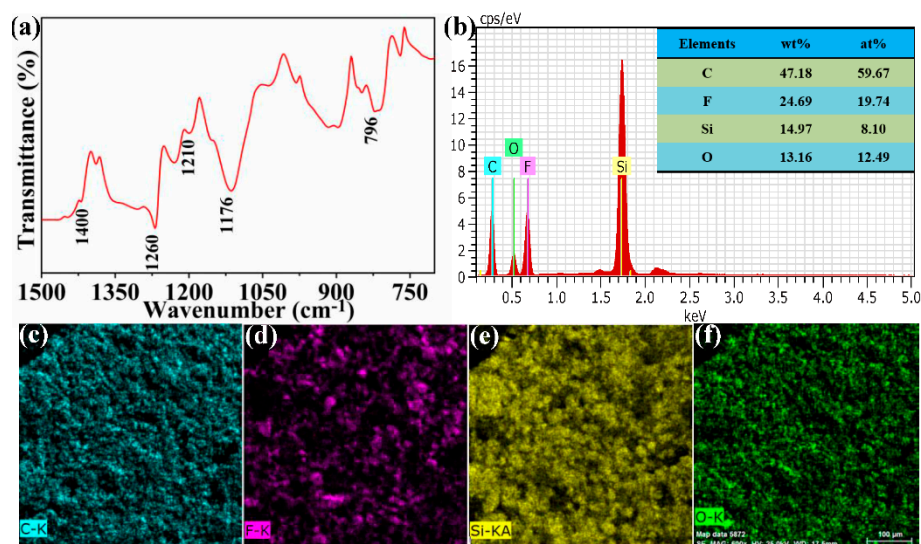


Figure 4. (a) FTIR spectra of the FCS coating; (b) EDS spectrum of the FCS coating (the inset shows the mass and atomic percentages of the FCS coating surface). Elemental distribution on the FCS coating surface (c–f).

3.2. Water Droplet Adhesion, Self-Cleaning and Anti-Fouling Properties

A facile method was adopted to measure water droplet adhesion on the FCS coating surface. As shown in Figure 5a,b, a $5\text{ }\mu\text{L}$ water droplet adhering to the needle moved vertically to the FCS coating surface and fully contacted the surface. After that, the water droplet was elongated as it moved upward (Figure 5c), which was attributed to the fact that the water droplet was embedded in the rough surface caused by curing. In Figure 5d, after the water droplet was completely separated from the surface, no residual droplet was found on it. In the droplet pinning test (Figure 5e,f), although the water droplet was also elongated due to adhesion between the water drop and rough surface, it can also be clearly seen that no residual droplet remained on the coating surface, indicating the low adhesion of the FCS coating surface.

Surface cleaning is very important for the practical application of flexible wearable materials, and self-cleaning surfaces have been proven to be effective in surface decontamination [45]. To test the self-cleaning property of the FCS coating, sand particles in a park were selected as contaminants. Figure 6a,c show images of sand particles on the PI surface and FCS coating, respectively. In the self-cleaning test, water droplets were continuously dropped onto the surface of sand pollutants by using a rubber tip dropper, and then changes in the surface cleaning property were observed. After the test, a large amount of sand contaminants still remained on the PI surface (Figure 6b). However, in contrast, water droplets with sand pollutants rolled down the FCS coating surface quickly, and soon the contaminants were all washed away from the surface by the water droplets, leaving a clean surface (Figure 6d). From the above analyses, it can be easily concluded that the FCS coating surface has excellent self-cleaning properties.

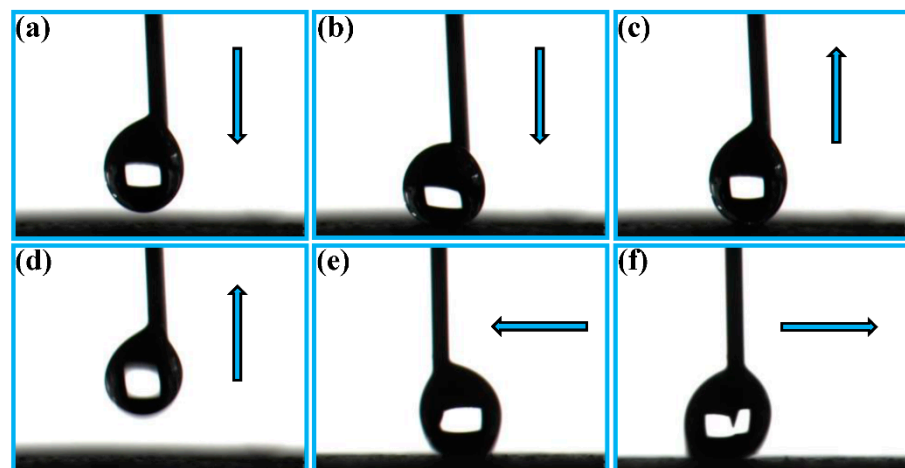


Figure 5. Water droplet adhesion test. Vertical droplet test (a–d) and droplet pinning test (e,f). Volume of a water droplet ($5 \mu\text{L}$).

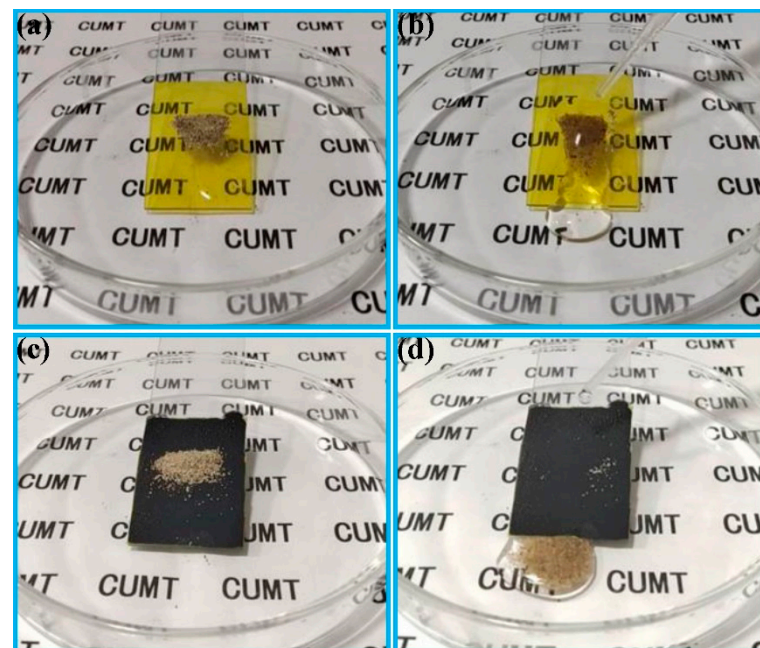


Figure 6. (a) Image of sand particles on the PI surface; (b) self-cleaning property of the PI surface; (c) image of sand particles on the FCS coating; and (d) self-cleaning property of the FCS coating.

In practical applications, the anti-fouling properties of flexible wearable materials to different contaminated fluids are closely related to the service life of materials. Here, corrosive waste polishing liquid and milk were selected to test the anti-fouling property of the FCS coating. Images of the PI surface and the FCS coating are displayed in Figure 7a,d. Figure 7b clearly shows that the corrosive polishing droplets flowed slowly through the surface as they dripped on the PI surface. After that, a large amount of residual liquid remained on the PI surface. Furthermore, a similar phenomenon was found when milk ran down the PI surface. For the FCS coating, as shown in Figure 7e,f, contaminated fluids displayed spherical shapes and rapidly rolled down the coating. No contaminated droplets were left on the surface, illustrating that the FCS coating has outstanding anti-fouling properties.

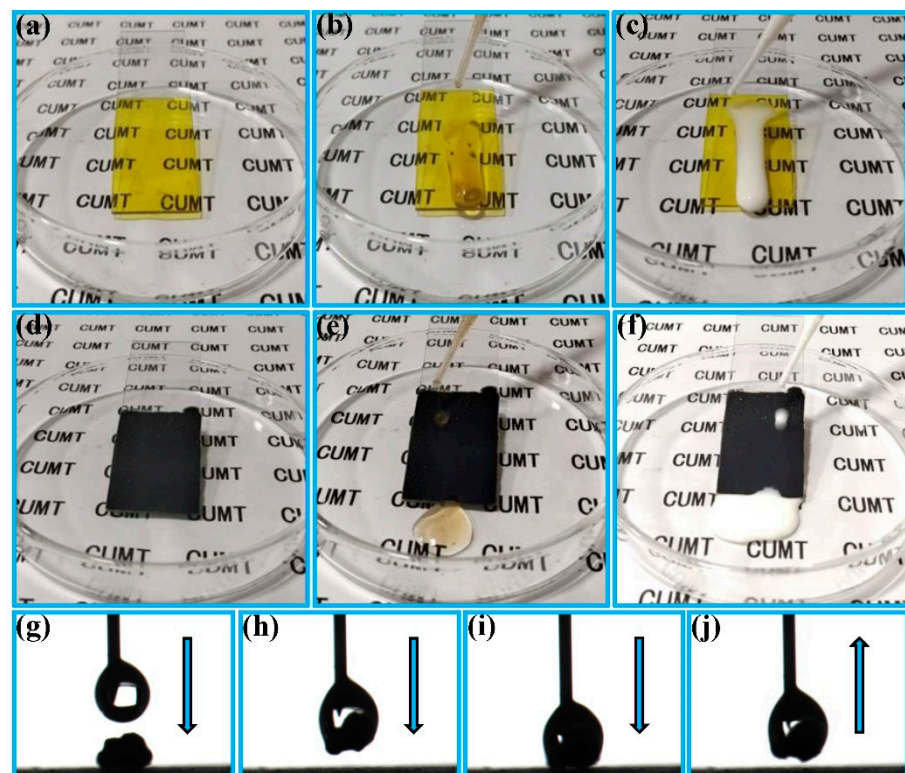


Figure 7. (a) Image of the PI surface. Anti-fouling properties of the PI surface demonstrated with different contaminated fluids (corrosive polishing waste liquid (b) and milk (c)); (d) image of the FCS coating. Anti-fouling properties of the FCS coating demonstrated with different contaminated fluids (corrosive polishing waste liquid (e) and milk (f)). Principle verification of the self-cleaning and anti-pollution properties of the FCS coating surface (g–j).

Many studies have been performed to explain the self-cleaning and anti-pollution mechanisms of superhydrophobic surfaces [46]. However, few experiments have been conducted to verify the mechanisms. The experimental verification process of self-cleaning mechanism is shown in Figure 7g–j. From Figure 7g, the droplet moved downward, closer to the sand particles. When the water droplet contacted the sand particles in Figure 7h, the sand particles were absorbed into the water droplet. After that, as the droplet moved to come into close contact with the FCS coating surface (Figure 7i) and then moved upward to separate from the FCS coating surface, no residual solution was found on the surface (Figure 7j), suggesting that the FCS coating surface has a low liquid adhesion property. Therefore, it can be concluded that the low surface adhesion force and the adsorption of water droplets on contaminated particles are the main factors affecting the self-cleaning and anti-fouling properties of superhydrophobic surfaces.

3.3. Durability

Flexible surfaces often bend and deform in applications. Therefore, it is very important to study the durability of superhydrophobic surfaces under different bending deformations. Furthermore, the durability of superhydrophobic surfaces is the basis of their large-scale industrial application. Movie S2 clearly shows that water droplets can still easily roll off the surface, even after rubbing by hand many times, showing the good superhydrophobic stability of the fabricated coating. Figure 8a shows the change in the wettability of the FCS surface at different numbers of bending cycles. Overall, with the increase in the number of bending cycles, the superhydrophobicity of the FCS coating worsens, showing that the WCA decreases and the SA increases. In particular, at 1700 bending cycles, an inflection point occurs in the variation of the FCS coating wettability, that is, the WCA curve drops sharply (the slope decreases), and the SA curve rises suddenly (the slope increases).

The above results can be attributed to the destruction of surface micro-nano structures during continuous bending. However, at 1900 bending cycles, the coating surface still remains superhydrophobic (152° WCA and 9.2° SA), which indicates that the FCS coating has good bending fatigue resistance. As the number of bending cycles increases to 2000, according to the definition of superhydrophobicity, the surface wettability changes from superhydrophobic to highly hydrophobic.

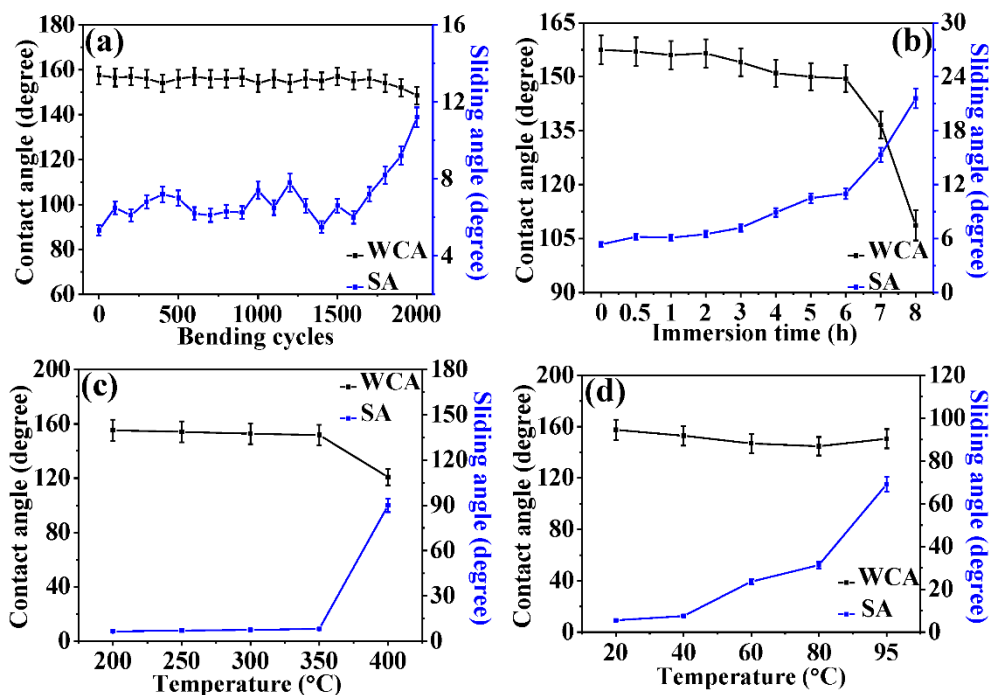


Figure 8. Change in the wettability of the FCS surface with different numbers of (a) bending cycles and (b) immersion time; (c) WCAs and SAs at different heating temperatures; (d) WCAs and SAs of water droplets ($5 \mu\text{L}$) at different temperatures.

In addition, the durability of the FCS coating surface immersed in deionized water was also studied in this work. In addition, the related results are displayed in Figure 8b. It can be easily observed that the WCA decreases and the SA increases with increasing immersion time, which suggests that the superhydrophobicity of the FCS coating surface gradually deteriorates. The FCS coating surface still maintains excellent hydrophobicity (149.5° WCA, 11° SA) after 6 h of immersion, proving that the obtained coating can maintain good superhydrophobic durability under water. As the immersion time increases to more than 6 h, at the same time, the fluctuation amplitudes of the WCAs (decrease) and SAs (increase) increase significantly. After 8 h of immersion, the WCA decreases to 108.7° and the SA increases to 21.6° . These above results are mainly caused by the hydrostatic pressure on the superhydrophobic surface. The corresponding detailed explanation can be obtained from Figure S3. Figure S3a displays the force analysis of the air layer trapped in the microstructure at the superhydrophobic interface. When the system is stable, a balance can be established between the hydrostatic pressure (P_G), air layer pressure (P_V) and suspension force generated by capillary force (P_H). The equilibrium relationship between the above three forces can be expressed by the following:

$$P_G = P_S = P_V + P_H \quad (5)$$

where P_V is related to temperature and air pressure, and P_H is determined by the length of the solid–liquid–gas three-phase contact line per unit area (Λ), solid–liquid contact area fraction (f_s), forward contact angle (θ_a) and liquid surface tension (γ_{LV}). Just as the sample is immersed in water, the coating surface of the sample is filled with an obvious air layer (as shown in Figure S3b). With increasing immersion time, more gas dissolved

in water and P_V decreased, which led to $P_G > P_S$; in addition, more liquid flowed into the surface microstructure (Figure S3c), which led to the coating surface superhydrophobicity to worsen with increasing immersion time. After a sufficiently long immersion time, a large amount of liquid permeated into the coating micro/nano structure (Figure S3c), making the FCS coating surface moist, which can explain why the surface hydrophobicity of the coating decreased faster after six hours of immersion.

The durability of the FCS coating at different heating temperatures is shown in Figure 8c. First, the samples were placed into a muffle furnace (PCD-C3000) and heated for 1 h at different temperatures. Then, the durability was evaluated by measuring the WCAs and SAs of each specimen. The results show that the FCS coating can maintain good superhydrophobicity when heated to 350 °C (151.8° WCA, 8.13° SA), indicating the excellent thermal stability of the coating. At 400 °C, the superhydrophobicity of the coating surface is destroyed (120.7° WCA, 90° SA), which can be explained by the thermal decomposition of PDMS and PVDF at 400 °C, and the coating surface loses the low surface energy necessary for superhydrophobicity. Due to capillary action between the surface microstructure and water droplet, the adhesion of water droplets on the surface increases, and the SA increases to 90°. At present, the measurement of surface wettability is mostly based on normal temperature water drops [47]. Hence, it is necessary to measure the wettability of water droplets at different temperatures, and the related results are displayed in Figure 8d. It can be easily found that the temperature of the water droplet has little effect on the WCAs, which decrease from 157.5° to 144.83°, but has a great influence on the SAs, which increase from 5.53° to 69.1°. The low surface energy of the coating is provided by stable intrinsic hydrophobic substances, and the surface structure and low surface energy of the coating are not damaged by high-temperature water drops. As a result, the droplet temperature has little effect on the WCAs of the coating surface. In addition, the temperature of the water droplet will heat the gas that filled the solid–liquid interface and accelerate the flow speed, which will lead to a decrease in the gas composition at the solid–liquid interface, and the liquid will penetrate into the microstructure, which results in a large increase in SAs.

3.4. Conductivity and Application

Bending deformation often occurs in human joint movement, such as finger bending, knee bending and ankle bending. In this work, the multifunctional FCS coating was taped to an index finger wearing a glove and used as an electronic sensor to detect finger motion in real time. At different bending angles, the corresponding normalized relative resistance ($\Delta R/R_0$) values can be obtained in the process of finger bending (as shown in Figure 9a). In the process of slow bending and the relaxation of the finger, it can be clearly found that the corresponding relative resistance values can be obtained at different bending angles, and the measured values show periodic changes, corresponding to the finger bending movement. The above results indicate that the flexible sensor can detect finger joint motion in real time. In human joint motion detection, every tiny change will cause a change in the sensor measurement results. Therefore, it is necessary to measure the mechanical sensitivity of sensors in harsh working conditions. Here, the FCS coating was wrapped on glass fiber rods with different diameters to measure the influence of the bending radius on its relative resistance. When the coating was bent, the bending strain resulted in an increase in the coating resistance. A higher bending radius was reflected by a larger $\Delta R/R_0$ value (Figure 9b), which is attributed to the fact that the bending tensile strain is large at a small bending radius, and the surface conductive path is greatly damaged. In Figure 9c, similar results can also be found in the sustained bending cycle test performed with different bending radii (1, 3 and 5 mm). Therefore, the reliability of the flexible sensor is evaluated by harsh bending fatigue tests. During the bending cycles, the real-time normalized resistance increased and decreased periodically with sustained bending and relaxation. After 600 continuous bending fatigue cycles, the resistance does not vary obviously, which indicates that the sensor has reliable mechanical stability. The obtained

coating is well adhered to the PI substrate, and the conductive path is not damaged, which is mainly attributed to the strong adhesion between the binder of the PI surface and the surface of the coating using PDMS as the binder.

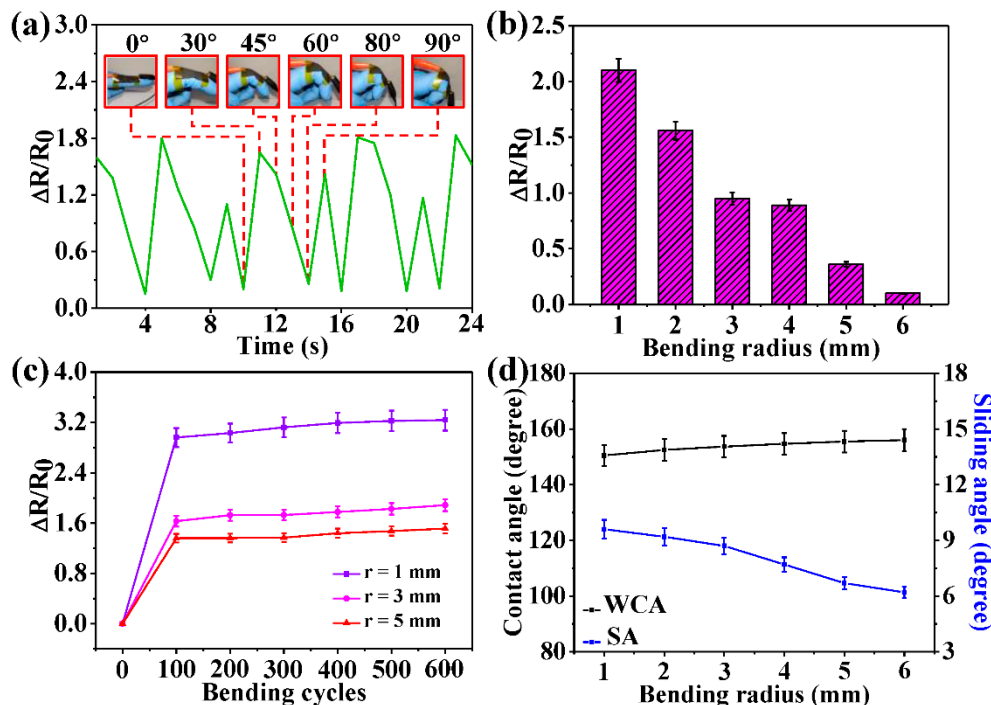


Figure 9. The obtained PI coating is used as an electronic sensor to detect human motion in real time: (a) the variation of $\Delta R/R_0$ with bending time, insets show digital photos of a finger with polyimide film sensors at different bending angles; (b) $\Delta R/R_0$ variation with different bending radii; (c) the change trend in $\Delta R/R_0$ values with the number of bending cycles performed with different bending radii. (d) The wettability of the flexible sensor surface after 600 bending cycles performed with different bending radii.

After that, by applying different bending radii, the change in the wettability of the flexible sensor surface after 600 bending cycles was reflected by measuring the WCAs and SAs. In Figure 9d, it is easily seen that a larger bending radius corresponds to a larger WCA and lower SA. The WCA changes from 150.5° to 156°, and the corresponding SA varies from 9.6° to 6.2°. Although the wettability decreased slightly, the surface remained superhydrophobic in the bending cycle range. The above results illustrate that the FCS coating can maintain stable superhydrophobicity during harsh bending fatigue cycling, which indicates that the obtained flexible sensor can work normally in dry or humid environments. Therefore, after further reasonable structural design, the FCS coating can be used as a wearable multifunctional sensor, such as a waterproof and wearable electronic device, to detect real-time physical signals in some humid environments.

4. Conclusions

In summary, a CNF/PVDF/PDMS conductive superhydrophobic coating was prepared on a PI substrate by several simple modifier-free one-step methods, and the resulting coating had a cauliflower-like microstructure. The obtained FCS coating possesses excellent superhydrophobicity to many kinds of droplets and has good self-cleaning and anti-fouling properties. Furthermore, the self-cleaning and anti-fouling properties of superhydrophobic surfaces are mainly determined by the low surface adhesion force and the adsorption of water droplets on contaminated particles. After multiple bending deformations, long immersion and high-temperature treatment, the fabricated coating still maintains stable superhydrophobicity. In addition, due to its reliable mechanical stability and superior sensitivity, the FCS coating is a good candidate for multifunctional smart sensors, and has

great application prospects in medical detection, waterproof flexible electrical devices and gesture detectors.

Supplementary Materials: The following are available online at <https://www.mdpi.com/2079-6412/11/1/95/s1>. Figure S1: Variations in the surface wettability, roughness and resistivity with different additive contents. Figure S2: Force analysis of the water droplet in the FCS coating microstructure and schematic diagram of gas–liquid interface changing with immersion time. Figure S3: (a) Force analysis of the water droplet in the FCS coating microstructure. Schematic diagram of the gas–liquid interface changing with immersion time (b,c). Table S1: The effect of CNF content on the surface resistivity. Table S2: The contact angle of water and diiodomethane on the polished FCS coating surface. The dispersion force and polarity force of water and diiodomethane. Movie S1: Wettability and water jet flow on the curved FCS coating surface. Movie S2: Variation of surface wettability after rubbing by hands.

Author Contributions: Conceptualization, methodology, writing—original draft preparation, validation, X.L.; data curation, writing—review and editing, K.C.; funding acquisition, D.Z. and Z.G. All authors have read and agreed to the published version of the manuscript.

Data Availability Statement: The data presented in this study are available in the article or supplementary material.

Acknowledgments: This work is supported by the National Nature Science Foundation of China (No. 51875564, 51675513 and 51735013) and the Priority Academic Program Development of Jiangsu Higher Education Institutions (PAPD).

Conflicts of Interest: The authors declare no conflict of interest.

References

1. Peng, J.; Zhao, X.; Wang, W.; Gong, X. Durable self-cleaning surfaces with superhydrophobic and highly oleophobic properties. *Langmuir* **2019**, *35*, 8404–8412. [[CrossRef](#)] [[PubMed](#)]
2. Song, M.; Hu, D.; Zheng, X.; Wang, L.; Yu, Z.; An, W.; Na, R.; Li, C.; Li, N.; Lu, Z. Enhancing droplet deposition on wired and curved superhydrophobic leaves. *ACS Nano* **2019**, *13*, 7966–7974. [[CrossRef](#)]
3. Ta, M.; Xu, F.; Ahmed, I.; Hou, X. One-step fabrication of superhydrophobic P(VDF-co-HFP) nanofibre membranes using electrospinning technique. *J. Appl. Polym. Sci.* **2019**, *48817*, 1–9.
4. Attia, H.; Johnson, D.; Wright, C.; Hilal, N. Robust superhydrophobic electrospun membrane fabricated by combination of electrospinning and electrospraying techniques for air gap membrane distillation. *Desalination* **2018**, *446*, 70–82. [[CrossRef](#)]
5. Vidal, K.; Gomez, E.; Goitandia, A.; Angulo-Ibanez, A.; Aranzabe, E. The synthesis of a superhydrophobic and thermal stable silica coating via sol-gel process. *Coatings* **2019**, *9*, 627. [[CrossRef](#)]
6. Su, X.; Li, H.; Lai, X.; Zhang, L.; Wang, J.; Liao, X.; Zeng, X. Vapor-liquid sol-gel approach to fabricating highly durable and robust superhydrophobic polydimethylsiloxane@silica surface on polyester textile for oil-water separation. *ACS Appl. Mater. Interfaces* **2017**, *9*, 28089–28099. [[CrossRef](#)]
7. Wang, S.; Wang, J. Anti-reflective and superhydrophobic films prepared from a sol at different withdrawal speeds. *Appl. Surf. Sci.* **2019**, *476*, 1035–1048. [[CrossRef](#)]
8. Qian, X.; Tang, T.; Wang, H.; Chen, C.; Luo, J.; Luo, D.L. Fabrication of hydrophobic Ni surface by chemical etching. *Materials* **2019**, *12*, 3546. [[CrossRef](#)]
9. Khodaei, M.; Shadmani, S. Superhydrophobicity on aluminum through reactive-etching and TEOS/GPTMS/nano-Al₂O₃ silane-based nanocomposite coating. *Surf. Coat. Technol.* **2019**, *374*, 1078–1090. [[CrossRef](#)]
10. Tuo, Y.; Zhang, H.; Rong, W.; Jiang, S.; Chen, W.; Liu, X. Drag reduction of anisotropic superhydrophobic surface prepared by laser etching. *Langmuir* **2019**, *35*, 11016–11022. [[CrossRef](#)]
11. Peng, C.; Wu, R.; Yang, Y.; Li, C.; Lin, Y.; Chen, S.; Kuai, Z.; Li, L. Hydrothermal formation of controllable hexagonal holes and Er₂O₃/Er₂O₃-RGO particles on silicon wafers toward superhydrophobic surfaces. *J. Colloid Interface Sci.* **2020**, *580*, 768–775. [[CrossRef](#)] [[PubMed](#)]
12. Li, X.; Chen, X.; Yi, Z.; Zhou, Z.; Tang, Y.; Yi, Y. Fabrication of ZnO nanorods with strong UV absorption and different hydrophobicity on foamed nickel under different hydrothermal conditions. *Micromachines* **2019**, *10*, 164. [[CrossRef](#)] [[PubMed](#)]
13. Celik, N.; Torun, I.; Ruzi, M.; Esidir, A.; Onses, M. Fabrication of robust superhydrophobic surfaces by one-step spray coating: Evaporation driven self-assembly of wax and nanoparticles into hierarchical structures. *Chem. Eng. J.* **2020**, *396*, 1–11. [[CrossRef](#)]
14. Abd El-Hady, M.; Sharaf, S.; Farouk, A. Highly hydrophobic and UV protective properties of cotton fabric using layer by layer self-assembly technique. *Cellulose* **2019**, *27*, 1099–1110. [[CrossRef](#)]
15. Xu, L.; Zhu, D.; Lu, X.; Lu, Q. Transparent, thermally and mechanically stable superhydrophobic coating prepared by an electrochemical template strategy. *J. Mater. Chem. A* **2015**, *3*, 3801–3807. [[CrossRef](#)]

16. Sun, J.; Li, Y.; Liu, G.; Chu, F.; Chen, C.; Zhang, Y.; Tian, H.; Song, Y. Patterning superhydrophobic area on a facile fabricated superhydrophilic layer based on inkjet printed water-soluble polymer template. *Langmuir* **2020**, *36*, 9952–9959. [[CrossRef](#)] [[PubMed](#)]
17. Li, D.; Fan, Y.; Han, G.; Guo, Z. Superomniphobic silk fibroin/Ag nanowires membrane for flexible and transparent electronic sensor. *ACS Appl. Mater. Interfaces* **2020**, *12*, 10039–10049. [[CrossRef](#)]
18. Liu, H.; Li, Q.; Bu, Y.; Zhang, N.; Wang, C.; Pan, C.; Mi, L.; Guo, Z.; Liu, C.; Shen, C. Stretchable conductive nonwoven fabrics with self-cleaning capability for tunable wearable strain sensor. *Nano Energy* **2019**, *66*, 1–9. [[CrossRef](#)]
19. Liu, S.; Zheng, J.; Hao, L.; Yegin, Y.; Bae, M.; Ulugun, B.; Taylor, T.; Scholar, E.; Cisneros-Zevallos, L.; Oh, J.; et al. Dual-functional, superhydrophobic coatings with bacterial anticontact and antimicrobial characteristics. *ACS Appl. Mater. Interfaces* **2020**, *12*, 21311–21321. [[CrossRef](#)]
20. Zhang, T.; Wang, D.; Liu, R.; Xie, Y.; Li, J.; Wang, L. A coral reef-like structure fabricated on cellulose paper for simultaneous oil-water separation and electromagnetic shielding protection. *ACS Omega* **2020**, *5*, 18105–18113. [[CrossRef](#)]
21. Han, G.; Nguyen, T.; Park, S.; Jung, Y.; Lee, J.; Lim, H. Moth-eye mimicking solid slippery glass surface with icephobicity, transparency, and self-healing. *ACS Nano* **2020**, *14*, 10198–10209. [[CrossRef](#)] [[PubMed](#)]
22. Sam, E.; Sam, D.; Lv, X.; Liu, B.; Xiao, X.; Gong, S.; Yu, W.; Chen, J.; Liu, J. Recent development in the fabrication of self-healing superhydrophobic surfaces. *Chem. Eng. J.* **2019**, *373*, 531–546.
23. Chen, Y.; Wang, L.; Wu, Z.; Luo, J.; Li, B.; Huang, X.; Xue, H.; Gao, J. Super-hydrophobic, durable and cost-effective carbon black/rubber composites for high performance strain sensors. *Compos. Part B-Eng.* **2019**, *176*, 1–10. [[CrossRef](#)]
24. Gao, J.; Wang, L.; Guo, Z.; Li, B.; Wang, H.; Luo, J.; Huang, X.; Xue, H. Flexible, superhydrophobic, and electrically conductive polymer nanofiber composite for multifunctional sensing applications. *Chem. Eng. J.* **2020**, *381*, 1–12. [[CrossRef](#)]
25. Ho, D.; Cheon, S.; Hong, P.; Park, J.; Suk, J.; Kim, D.; Han, J. Multifunctional smart textronics with blowlogpun nonwoven fabrics. *Adv. Funct. Mater.* **2019**, *29*, 1–9. [[CrossRef](#)]
26. Su, X.; Li, H.; Lai, X.; Chen, Z.; Zeng, X. 3D porous superhydrophobic CNT/EVA composites for recoverable shape reconfiguration and underwater vibration detection. *Adv. Funct. Mater.* **2019**, *29*, 1–11. [[CrossRef](#)]
27. Xu, R.; Zhang, K.; Xu, X.; He, M.; Lu, F.; Su, B. Superhydrophobic WS₂-nanosheet-wrapped sponges for underwater detection of tiny vibration. *Adv. Sci.* **2018**, *5*, 1–10. [[CrossRef](#)]
28. Das, S.; Srinivasan, S.; Stromberg, L.; He, Q.; Garland, N.; Straszheim, W.; Ajayan, P.; Balasubramanian, G.; Claussen, J. Superhydrophobic inkjet printed flexible graphene circuits via direct-pulsed laser writing. *Nanoscale* **2017**, *9*, 19058–19065. [[CrossRef](#)]
29. Gustafsson, L.; Jansson, R.; Hedhammar, M.; van der Wijngaart, W. Structuring of functional spider silk wires, coatings, and sheets by self-assembly on superhydrophobic pillar surfaces. *Adv. Mater.* **2017**, *30*, 1–8. [[CrossRef](#)]
30. Liu, X.; Zhang, D.; Guo, Z. A facile modifier-free approach to fabricate antistatic superhydrophobic composite coatings with remarkable thermal stability and corrosion resistance. *J. Bionic Eng.* **2020**, *17*, 421–435. [[CrossRef](#)]
31. Li, L.; Bai, Y.; Li, L.; Wang, S.; Zhang, T. A superhydrophobic smart coating for flexible and wearable sensing electronics. *Adv. Mater.* **2017**, *19*, 1–8. [[CrossRef](#)] [[PubMed](#)]
32. Su, X.; Li, H.; Lai, X.; Chen, Z.; Zeng, X. Highly stretchable and conductive superhydrophobic coating for flexible electronics. *ACS Appl. Mater. Interfaces* **2018**, *10*, 10587–10597. [[CrossRef](#)] [[PubMed](#)]
33. Xu, H.; Fan, S.; Lu, Y.; Feng, H.; Qiu, J. Proposal and verification of a novel superhydrophobic-conductive anti-corrosion polyaniline-silica coating. *Bull. Chem. Soc. Jpn.* **2020**, *93*, 1114–1120. [[CrossRef](#)]
34. Song, B.; Li, J.; Wu, F.; Patel, S.; Hah, J.; Wang, X.; Moon, K.; Wong, C. Processing and characterization of silver-filled conductive polysulfide sealants for aerospace applications. *Soft Matter* **2018**, *14*, 9036–9043. [[CrossRef](#)]
35. Saddiqi, N.; Seeger, S. Chemically resistant, electric conductive, and superhydrophobic coatings. *Adv. Mater. Interfaces* **2019**, *9*, 1–9. [[CrossRef](#)]
36. Hong, T.; Jeong, S.; Choi, Y.; Lim, T.; Ju, S. Superhydrophobic, elastic, and conducting polyurethane-carbon nanotube-silane-aerogel composite microfiber. *Polymers* **2020**, *12*, 1772. [[CrossRef](#)]
37. Lu, Y.; Sathasivam, S.; Song, J.; Crick, C.R.; Carmalt, C.J.; Parkin, I. Robust self-cleaning surfaces that function when exposed to either air or oil. *Science* **2015**, *347*, 1132–1135. [[CrossRef](#)]
38. Das, A.; Megaridis, C.; Liu, L.; Wang, T.; Biswas, A. Design and synthesis of superhydrophobic carbon nanofiber composite coatings for terahertz frequency shielding and attenuation. *Appl. Phys. Lett.* **2011**, *98*, 1–3. [[CrossRef](#)]
39. Baldelli, A.; Ou, J.; Barona, D.; Li, W.; Amirfazli, A. Sprayable, superhydrophobic, electrically, and thermally conductive coating. *Adv. Mater. Interfaces* **2020**, *19*, 1–9. [[CrossRef](#)]
40. Liao, X.; Li, H.; Lai, X.; Chen, W.; Zeng, X. Facile fabrication of superhydrophobic conductive polydimethylsiloxane@silver nanowires cotton fabric via dipping-thermal curing method. *Mater. Lett.* **2019**, *255*, 1–4. [[CrossRef](#)]
41. Chen, K.; Gou, W.; Xu, L.; Zhao, Y. Low cost and facile preparation of robust multifunctional coatings with self-healing superhydrophobicity and high conductivity. *Compos. Sci. Technol.* **2018**, *156*, 177–185. [[CrossRef](#)]
42. Yin, X.; Yu, S.; Bi, X.; Liu, E.; Zhao, Y. Robust superhydrophobic 1D Ni₃S₂ nanorods coating for self-cleaning and anti-scaling. *Ceram. Int.* **2019**, *45*, 24618–24624. [[CrossRef](#)]

43. Zhong, A.; Li, J.; Zhang, Y.; Zhang, F.; Wang, T.; Zhang, G.; Sun, R.; Wong, C. Low temperature microwave fabrication of three-dimensional graphene/polyimide foams with flexibility strain responsivity. *Compos. Part A-Apl. Sci. Manuf.* **2020**, *137*, 1–10. [[CrossRef](#)]
44. Owens, D.; Wendt, R. Estimation of the surface free energy of polymers. *J. Appl. Polym. Sci.* **1969**, *13*, 1741–1747. [[CrossRef](#)]
45. Aktij, S.; Taghipour, A.; Rahimpour, A.; Mollahosseini, A.; Tiraferri, A. A critical review on ultrasonic-assisted fouling control and cleaning of fouled membranes. *Ultrasonics* **2020**, *108*, 1–20.
46. Li, J.; Wei, Y.; Huang, Z.; Wang, F.; Yan, X.; Wu, Z. Electrohydrodynamic behavior of water droplets on a horizontal super hydrophobic surface and its self-cleaning application. *Appl. Surf. Sci.* **2017**, *403*, 133–140. [[CrossRef](#)]
47. Qi, W.; Li, J.; Weisensee, P. Evaporation of sessile water droplets on horizontal and vertical bi-philic patterned surfaces. *Langmuir* **2019**, *35*, 17185–17192. [[CrossRef](#)]